Supporting Information

Expanding COF Layer Stacking Distances for Enhanced Photocatalytic Activity

Jiyuan Zang,[†] Haiqin Liu,[†] David J. Young,[‡] Zhi-Gang Ren,[†] and Hong-Xi Li[†]*

[†]College of Chemistry, Chemical Engineering and Materials Science, Soochow University, Suzhou 215123, People's Republic of China

[‡]James Watt School of Engineering, University of Glasgow, University Avenue, Glasgow, G12 8QQ UK

E-mail: lihx@suda.edu.cn (H.-X.L.)

Materials.

All chemicals used were of analytical grade. Phenyl isothiocyanate (PhCNS) was purchased from Macklin Inc. (Shanghai, China; purity greater than 99.5%). p-Phenylenediamine (Pa) and nickel (II) acetylacetonate were purchased from Aladdin Chemistry Co. Ltd. (Shanghai, China; purity greater than 95%). 1,3,5-triformyl phloroglucinol (Tp) was purchased from Adamas-beta (Shanghai, China; purity greater than 98%).

Characterization.

Powder X-ray diffraction (PXRD) patterns were obtained with a Bruker AXS D8 Advanced SWAX diffractometer using Cu-Kα (0.15406 nm) radiation. Fourier transform infrared spectra (FT-IR) were recorded on a Bruker VERTEX 70 + HYPERION 2000. ^{1}H nuclear magnetic resonance (NMR) spectra were recorded on a Bruker 400 M NMR spectrometer, the solid state ^{13}CNMR spectra were recorded on a 400 MHz Brucker AVANCEIII/WB-400 spectrometer. The scanning electron microscopy (SEM) images were obtained on a HITACHI S-4700 field-emission scanning electron microscope, transmission electron microscopy (TEM) images were obtained using a Hitachi HT770 transmission electron microscope. X-ray photoelectron spectra (XPS) were recorded with an X-ray photoelectron spectrometer (ESCALAB Xi+, USA) whose binding energies were referenced to C 1s at 284.8 eV from hydrocarbon to compensate charging effect. UV-vis spectra were obtained with a Shimadzu UV-2600 spectrometer. The specific surface area and pore structure were determined by N_2 adsorption-desorption measurements at 77K using a gas sorption analyzer (Si-2MP, Anton Paar, Austria). The specific surface area was calculated using the Brunauer–Emmett–Teller (BET) method from the adsorption data in the relative pressure (P/P_0) range of 0.05–0.30. X-ray absorption fine structure (XAFS) spectroscopy at the Ni K-edge was performed using a laboratory-scale XAFS spectrometer (RapidXAFS 2M, Anhui Absorption Spectroscopy Analysis Instrument Co., Ltd.) operated at 20 kV and 20 mA. The measurements were conducted in transmission mode. A Si (111) double-crystal monochromator was used to scan the incident X-ray energy across the absorption edge.

Photocatalytic H_2 evolution.

A flask fitted with a quartz filter (200 mL) was charged with 2 mg of sample, 300 mg of sodium ascorbate (SA) as the sacrificial agent and 50 mL of PBS (phosphate buffered saline, 0.2 M, pH=7) buffer solution, and then sonicated for 30 min to disperse it evenly. Prior to the photocatalytic test, the device was evacuated several times. It was then connected to a glass automatic on-line trace gas analysis system (Labsolar-6A, Beijing Perfect Light Technology Co., Ltd, China). The reaction was irradiated with a 300 W xenon lamp, which had a cutoff wavelength of 420 nm, and the temperature was maintained at 25 °C using water cooling. The amount of evolved H_2 was periodically measured using online gas chromatography (GC7900, Tianmei, China).

Photoelectrochemical characterization.

Electrochemical impedance spectroscopy (EIS) and transient photocurrent measurements were obtained on an electrochemical analyzer (CHI760E Instruments) with a conventional three-electrode cell with Pt wire as the counter electrode, Ag/AgCl as a reference electrode and 0.1 mol L^{-1} Na_2SO_4 as the electrolyte. The working electrode was prepared by spreading sample (1 mg mL^{-1} in isopropanol with 32 μL 5 wt% Nafion) on F-doped tin oxide glass. The light source was a xenon lamp (300 W) with a 420 nm cut-off filter.

Apparent quantum efficiency (AQE) measurements.

AQE for H_2 evolution was measured under the illumination of a xenon lamp (300 W) with different bandpass filters of 420 ± 10 nm, 475 ± 10 nm, 500 ± 10 nm, and 550 ± 10 nm with intensities of 0.61, 0.50, 0.38 and 0.50 mW·cm^{-2}, respectively. Samples were suspended in PBS (50 mL) with SA (300 mg). The irradiation area was confined to 3.14 × 3 cm^2. The value of AQE was calculated according to the following equation:

$$\eta_{AQE} = \frac{N_e}{N_p} \times 100\%$$

$$= \frac{2 \times \eta \times N_A}{\frac{E_{total}}{E_{photon}}} \times 100\%$$

$$E_{total} = S \times P \times t$$

$$E_{photon} = h \times \frac{c}{\lambda}$$

$$\eta_{AQE} = \frac{2 \times n \times N_A \times h \times c}{S \times P \times t \times \lambda} \times 100\%$$

where N_e is the number of generated electrons for H_2, N_p is the number of incident photons, n is the molar mass of H_2 molecules produced over 1 hour (mol), N_A (Avogadro constant) = 6.022×10^{23} mol^{-1}, h (the Planck's constant) = 6.626×10^{-34} J·s, c (the light speed) = 3×10^8 $m \cdot s^{-1}$, S (the irradiation area) = 38 cm^2, P is the intensity of irradiation light ($W \cdot cm^{-2}$), t (the photoreaction time) = 3600 s, λ is the wavelength of the monochromatic light (4.20×10^{-7}, 4.75×10^{-7}, 5.00×10^{-7}, or 5.50×10^{-7}m).

Computational methods.

Modeling of COF was performed using the Material Studio software.[1] Density functional theory (DFT) calculations were carried out using the B3LYP hybrid functional.[2] The optimized configuration was confirmed as an energy minimum with no imaginary frequencies in the vibrational analysis, and this stable structure was subsequently used for electronic structure and property calculations. The adsorption free energy for a H atom on a substrate was calculated using the model of Nørskov et al.:[3]

$$\Delta G_H = \Delta E_H + \Delta E_{ZPE} - T\Delta S$$

where ΔEZPE and ΔS are the changes of zero-point energy and entropy, T is the absolute temperature. $\Delta E_{ZPE} - T\Delta S \approx 0.26$ eV is generally used for HER. ΔE_H denotes the adsorption energy of a hydrogen atom on a substrate and was calculated by:

$$\Delta E_H = E(sub/H) - E(sub) - E(H_2)/2$$

where E(sub/H), E(sub) and $E(H_2)$ are the total energies of a H atom on a substrate, substrate alone and hydrogen gas, respectively.

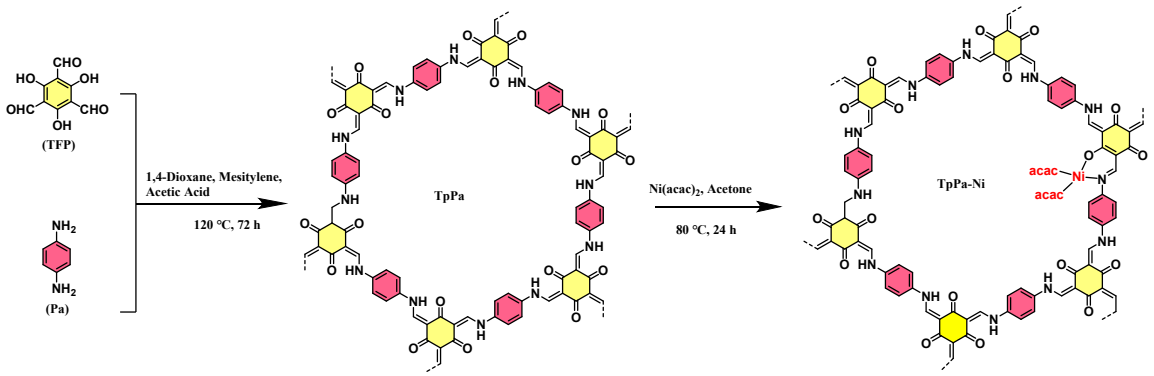

Scheme S1 Synthesis of TpPa and TpPa-Ni.

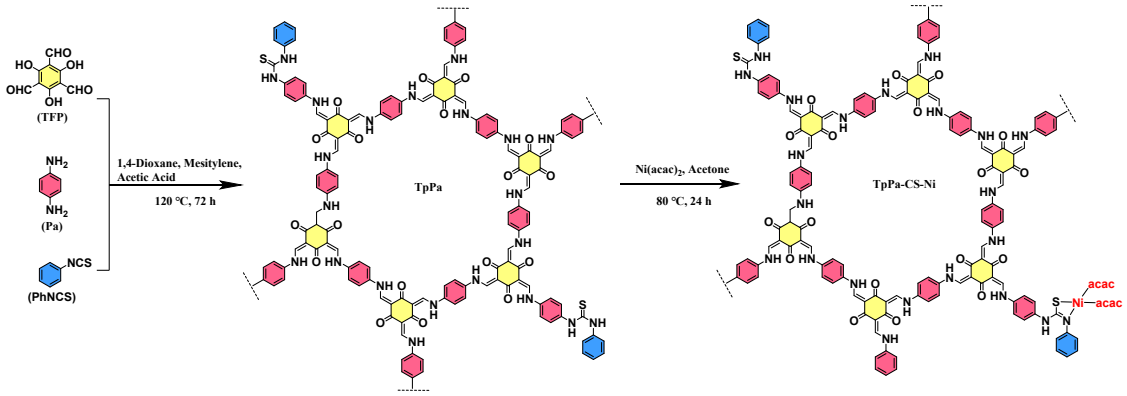

Scheme S2 Synthesis of TpPa-CS and TpPa-CS-Ni.

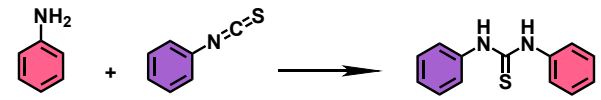

Scheme S3 Synthesis of N,N'-Diphenylthiourea ($(PhNH)_2CS$).

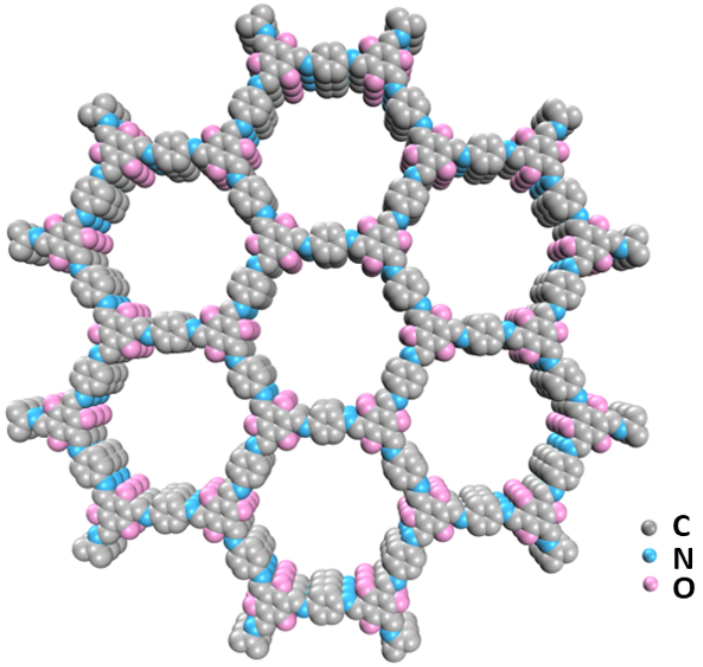

Fig. S1 Simulated structures of TpPa.

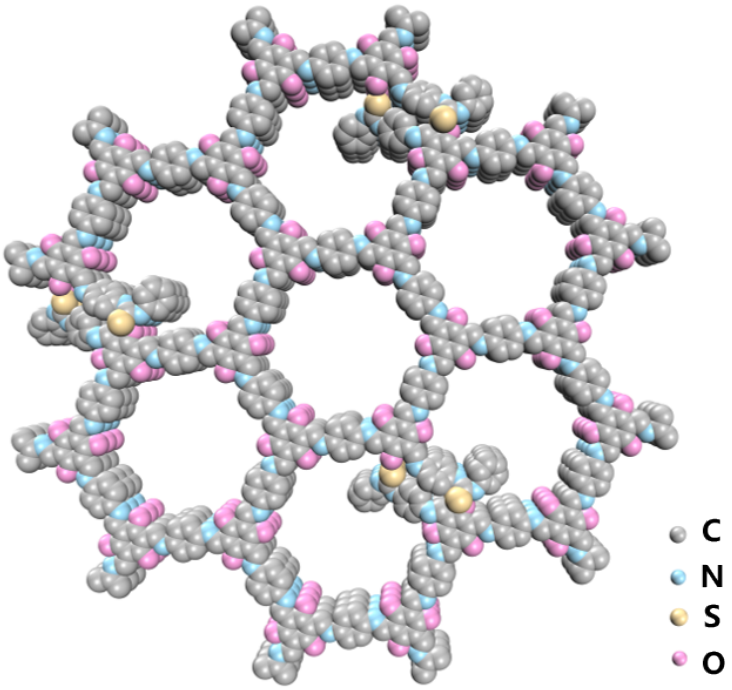

Fig. S2 Simulated structures of TpPa-CS.

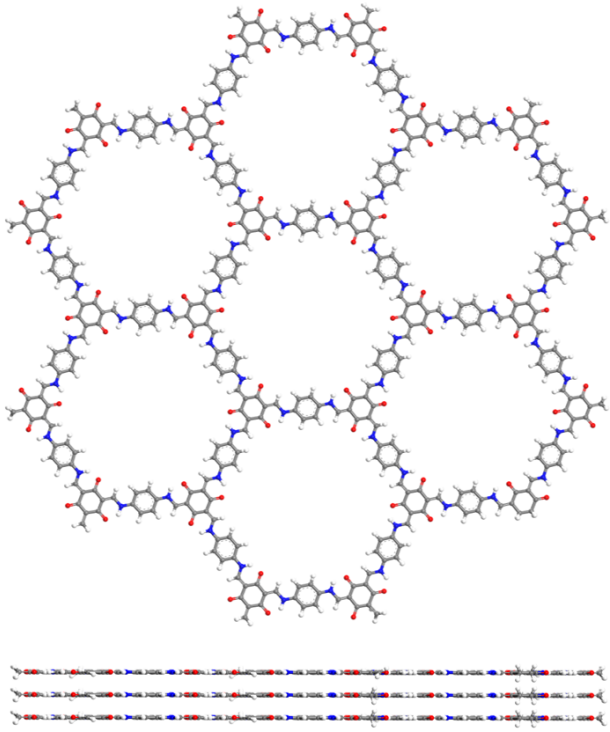

Fig. S3 The AA stacking mode of TpPa simulated by Material Studio.

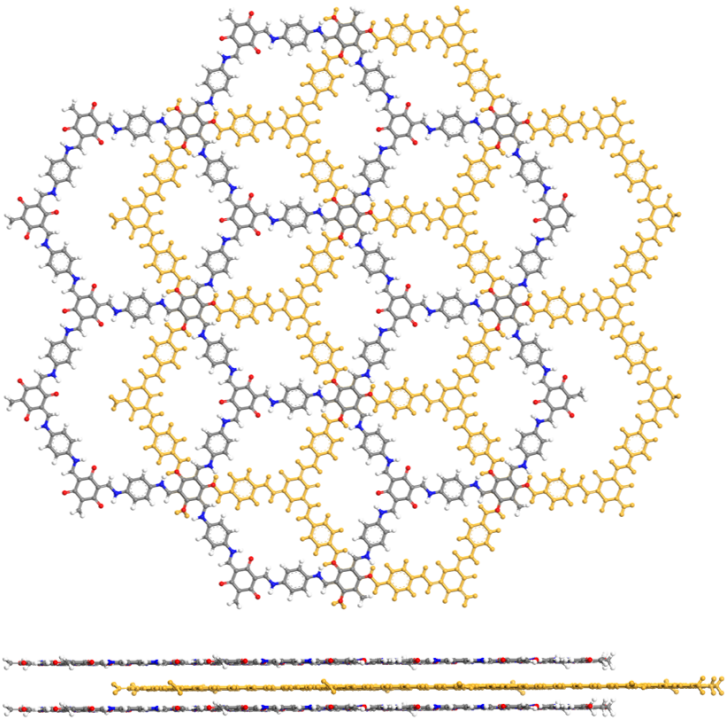

Fig. S4 The AB stacking mode of TpPa simulated by Material Studio.

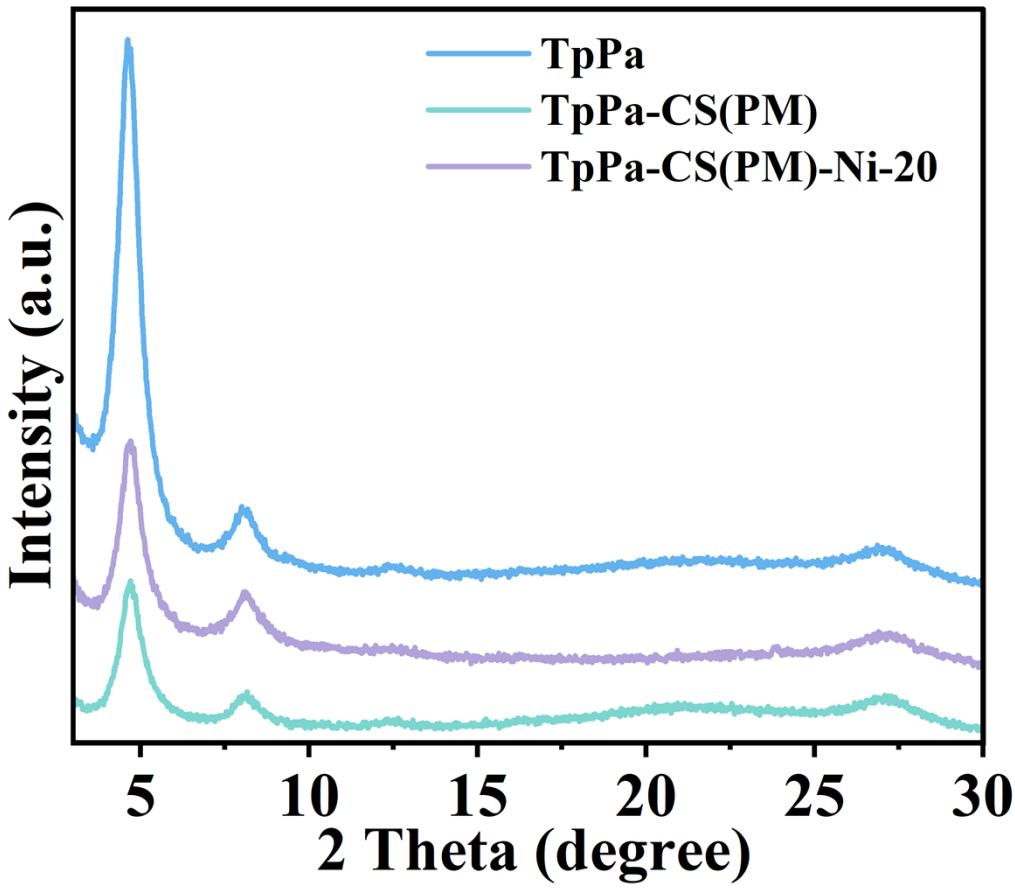

Fig. S5 TpPa-CS(PM) and TpPa-CS(PM)-Ni-20.

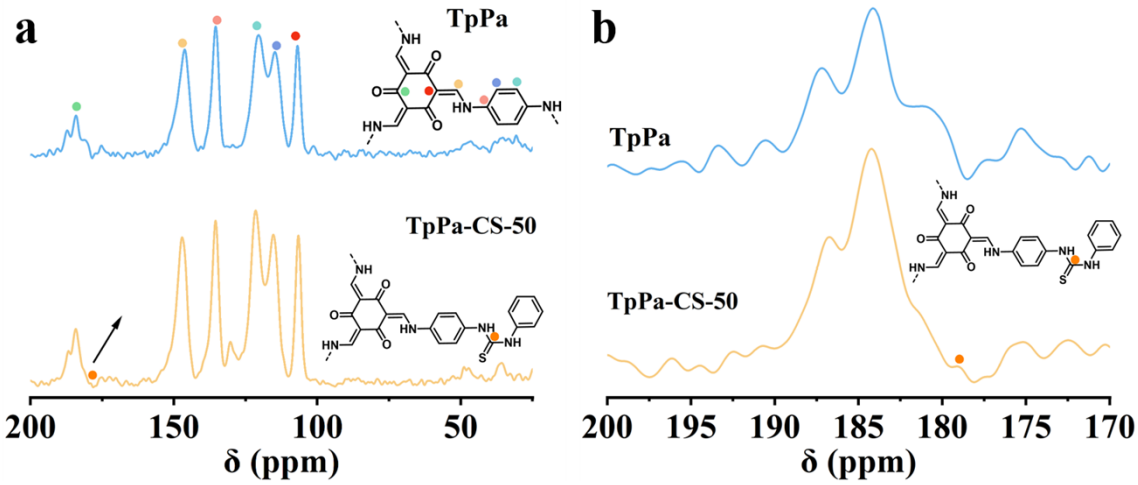

Fig. S6 Solid-state ^{13}C NMR spectra of TpPa and TpPa-CS-50.

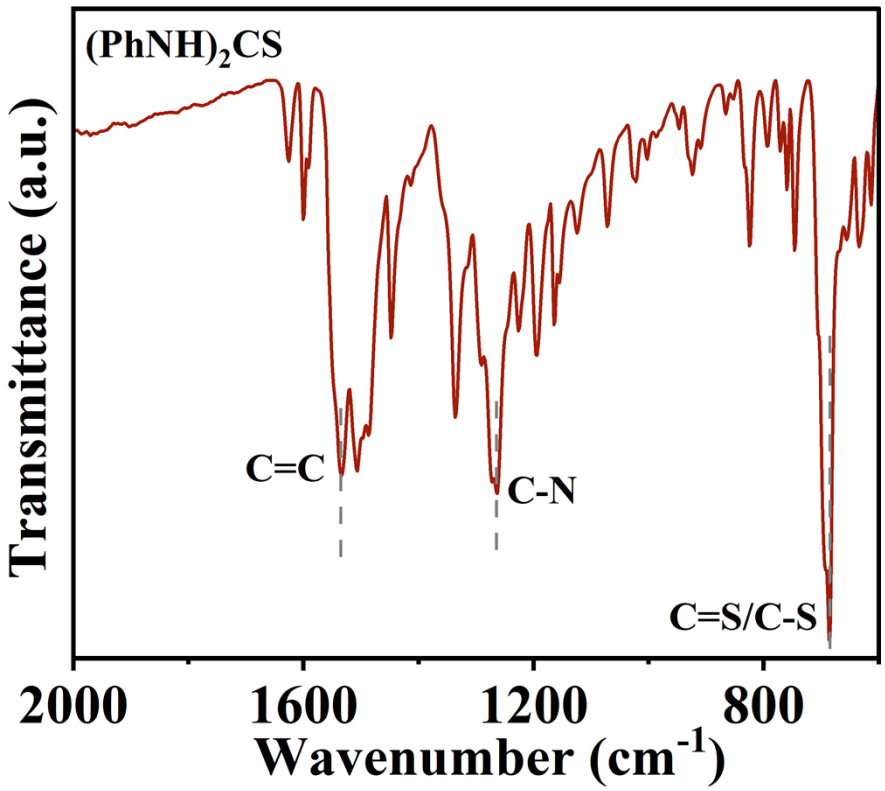

Fig. S7 FT-IR spectrum of $(PhNH)_2CS$.

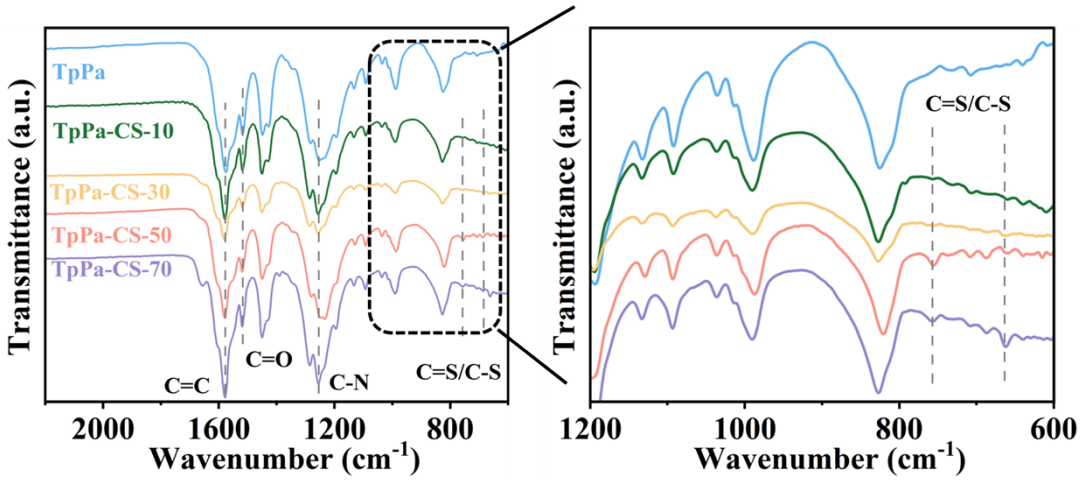

Fig. S8 FT-IR spectra of TpPa-CS-X (X =0, 10, 30, 50 and 70).

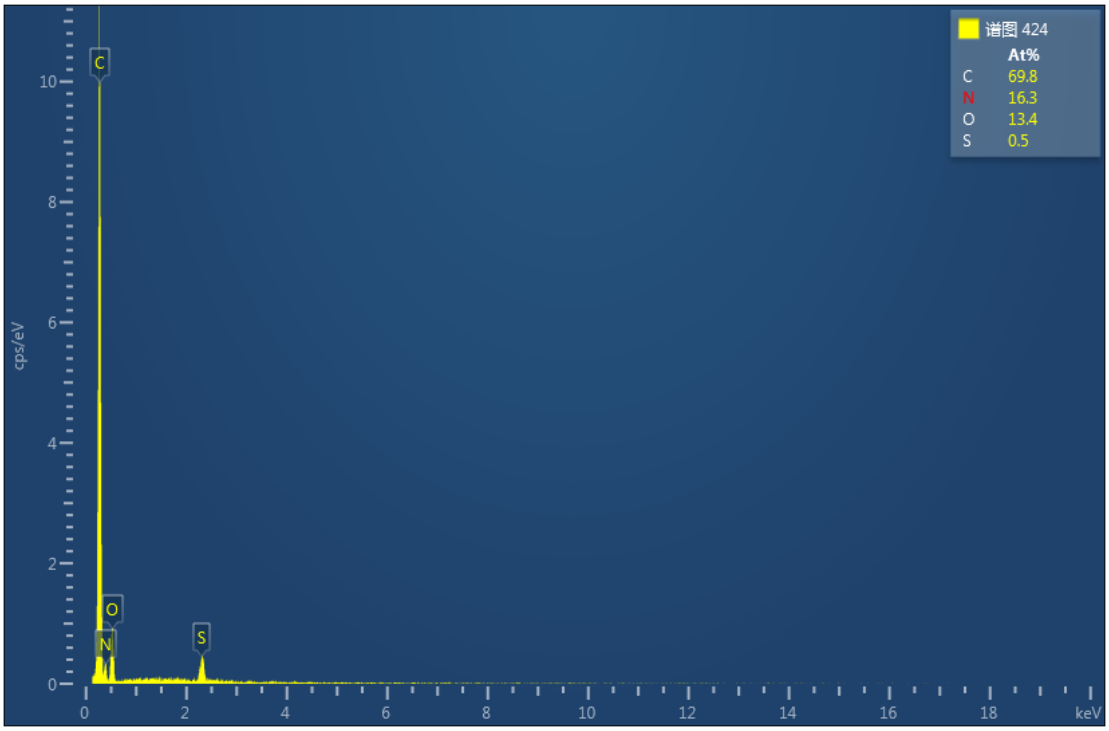

Fig. S9 EDS spectrum of TpPa-CS-10.

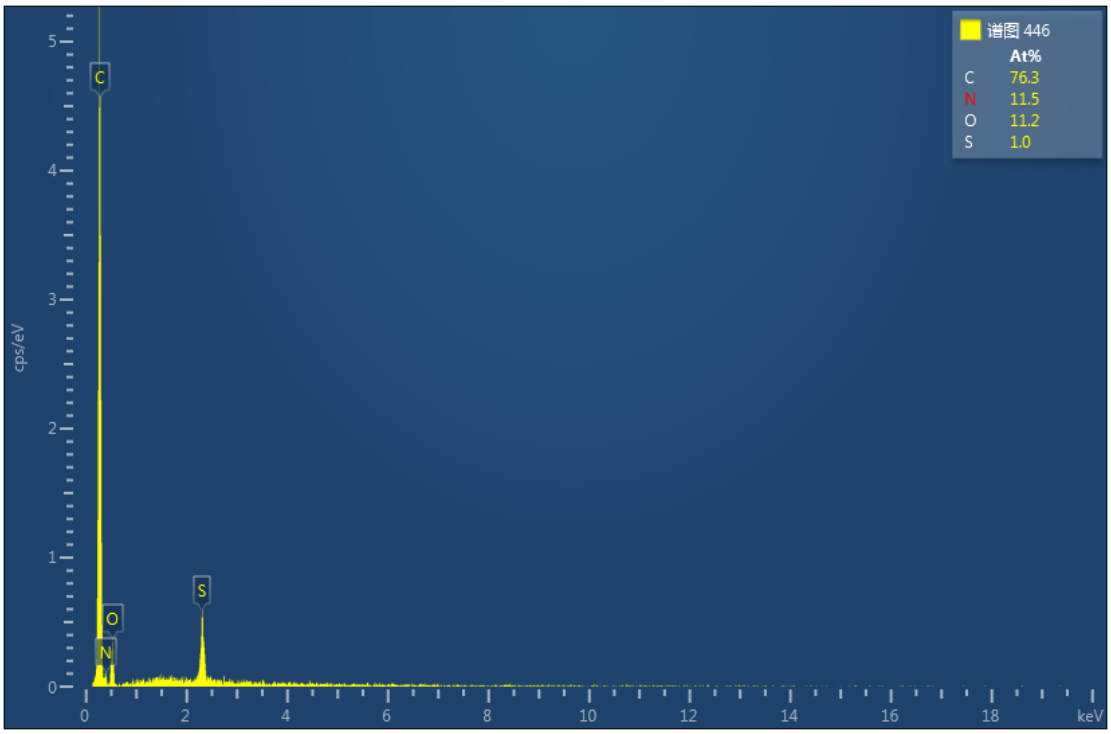

Fig. S10 EDS spectrum of TpPa-CS-30.

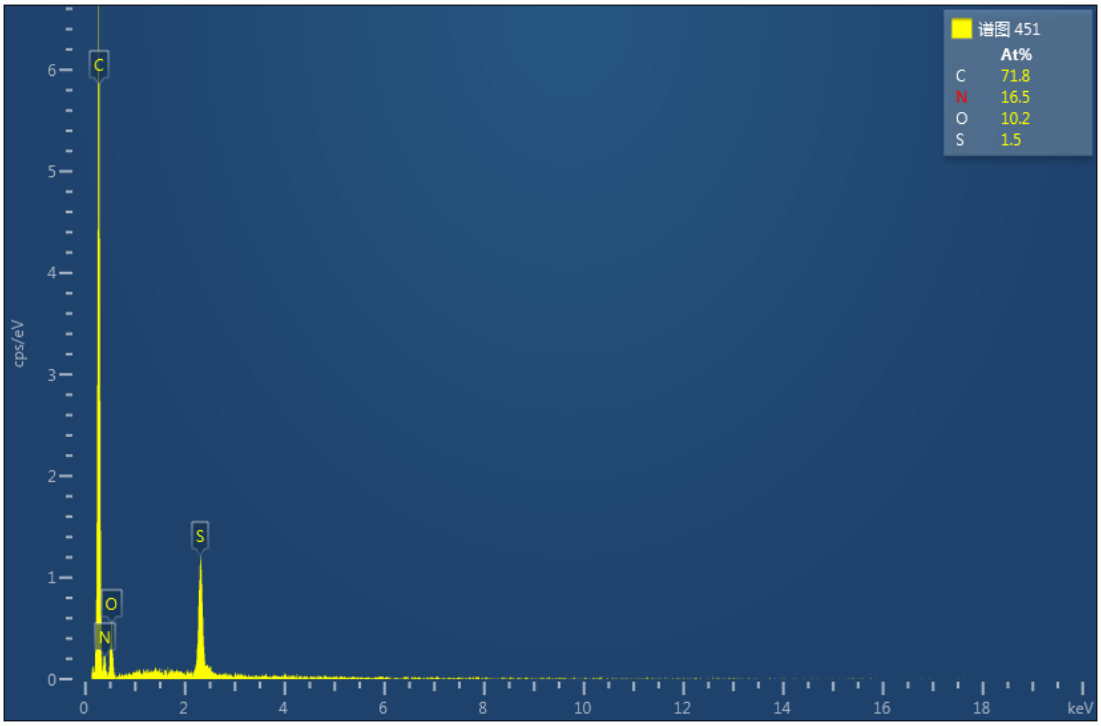

Fig. S11 EDS spectrum of TpPa-CS-50.

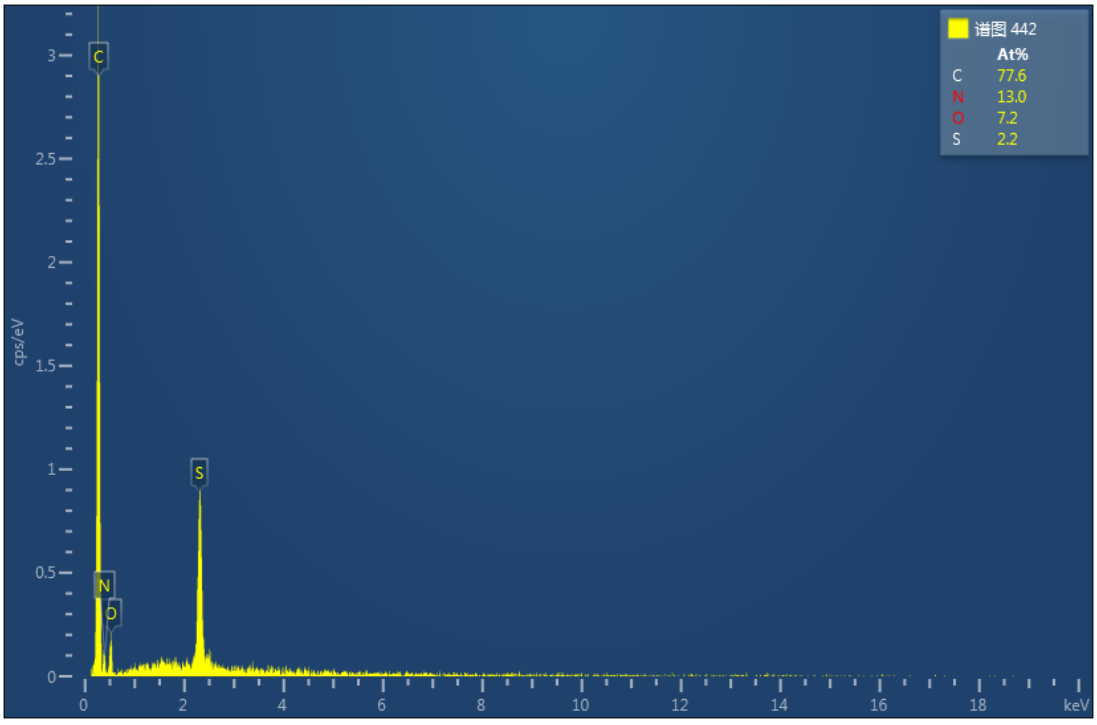

Fig. S12 EDS spectrum of TpPa-CS-70.

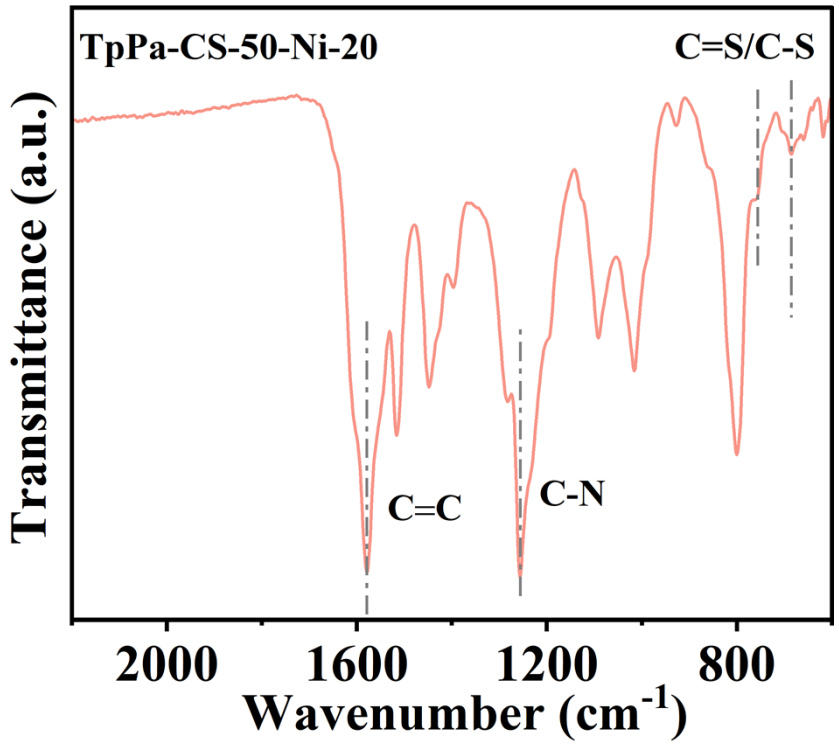

Fig. S13 FT-IR spectrum of TpPa-CS-50-Ni-20.

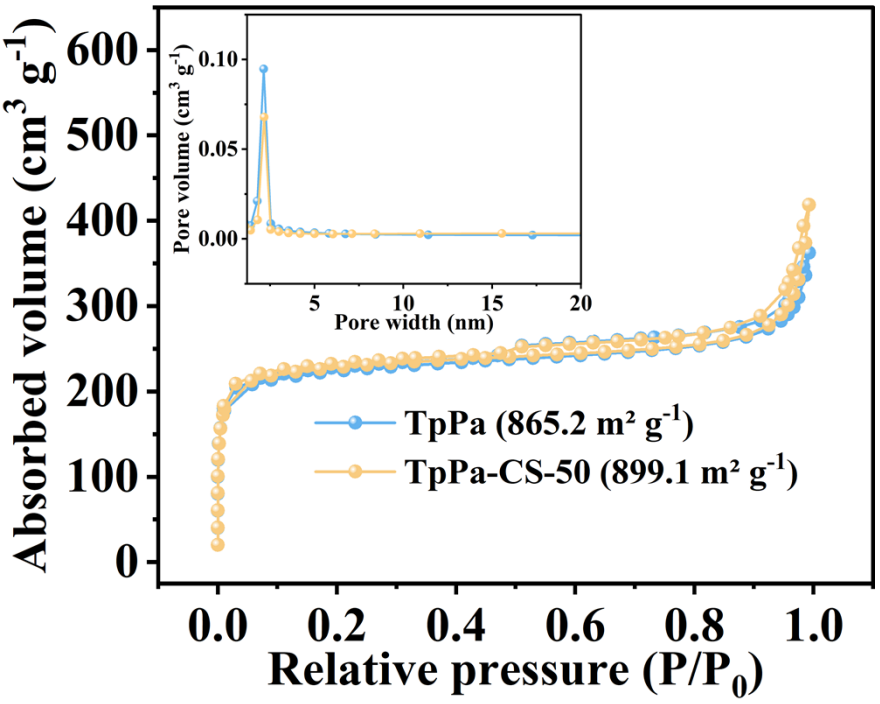

Fig. S14 N_2 adsorption/desorption isotherms (pore-size distribution in the illustration) of TpPa and TpPa-CS-50.

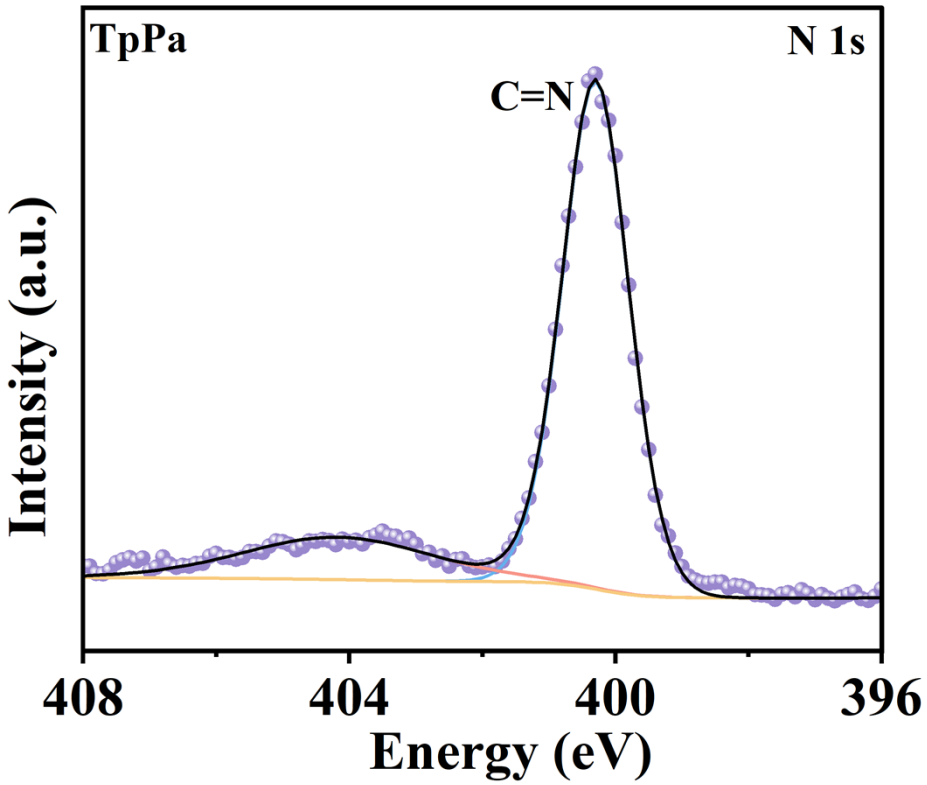

Fig. S15 XPS spectrum of N 1s of TpPa.

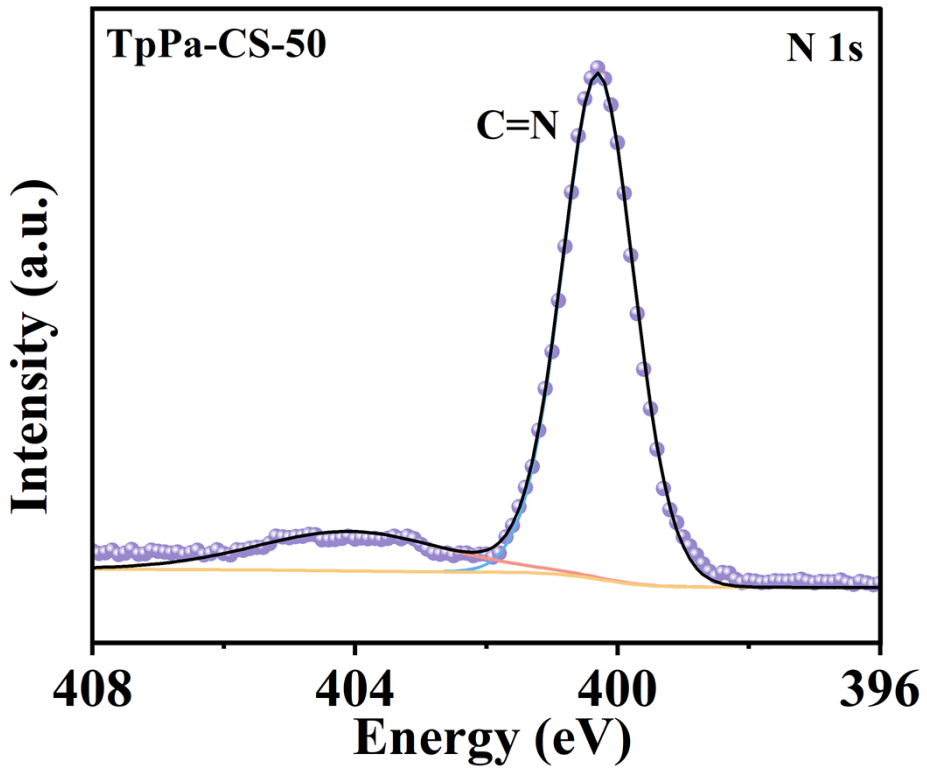

Fig. S16 XPS spectrum of N 1s of TpPa-CS-50.

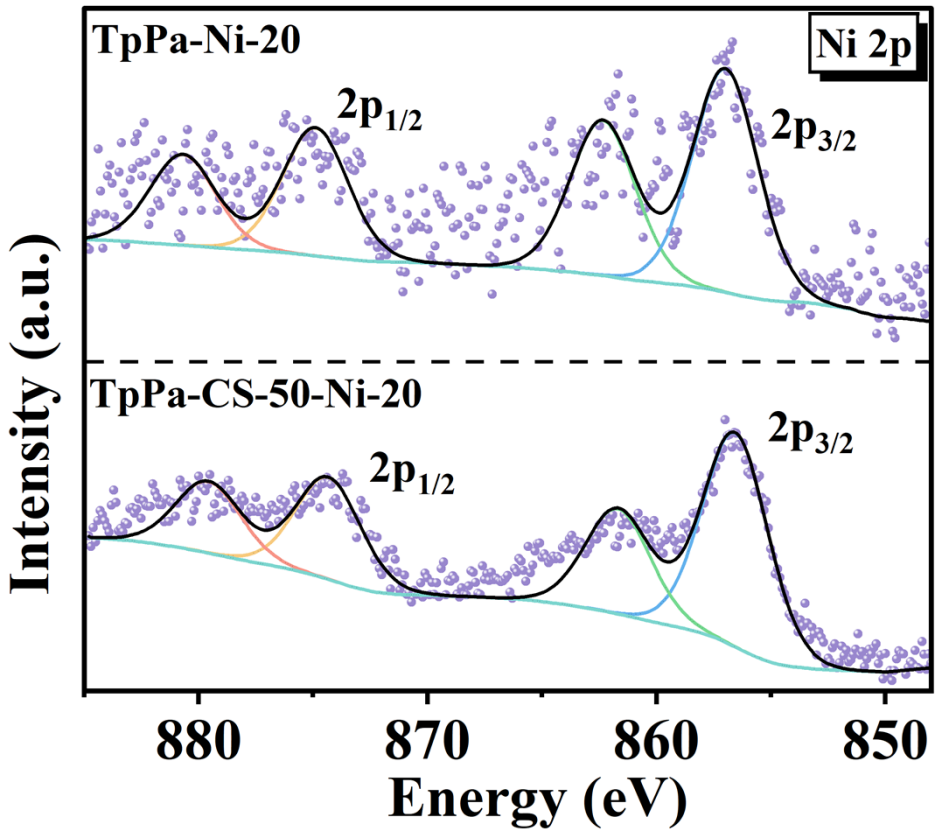

Fig. S17 XPS spectrum of Ni 2p of TpPa-Ni-20 and TpPa-CS-50-Ni-20.

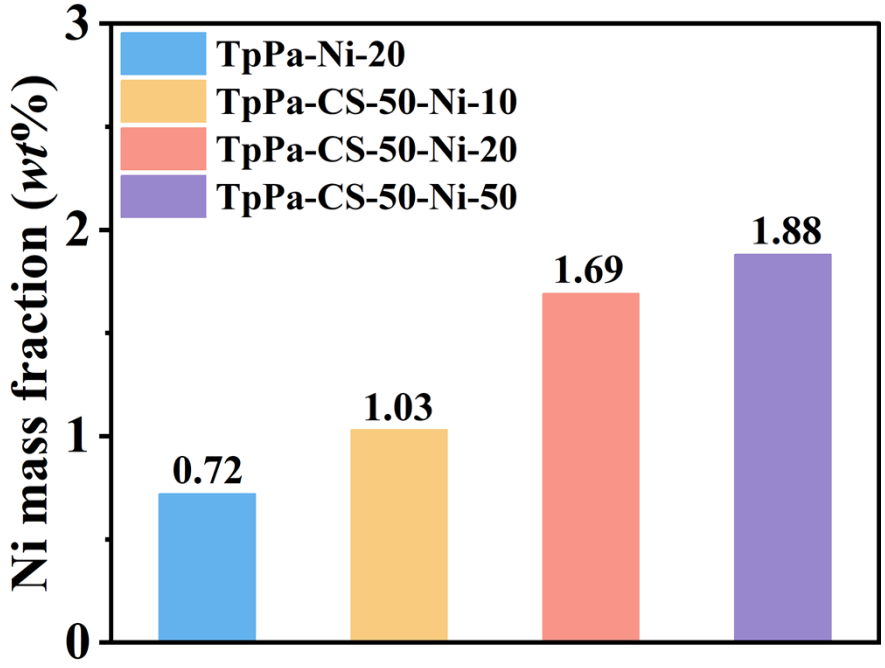

Fig. S18 ICP data of the loaded Ni content of TpPa-Ni-20 and TpPa-CS-50-Ni-X (X = 10, 20 and 50).

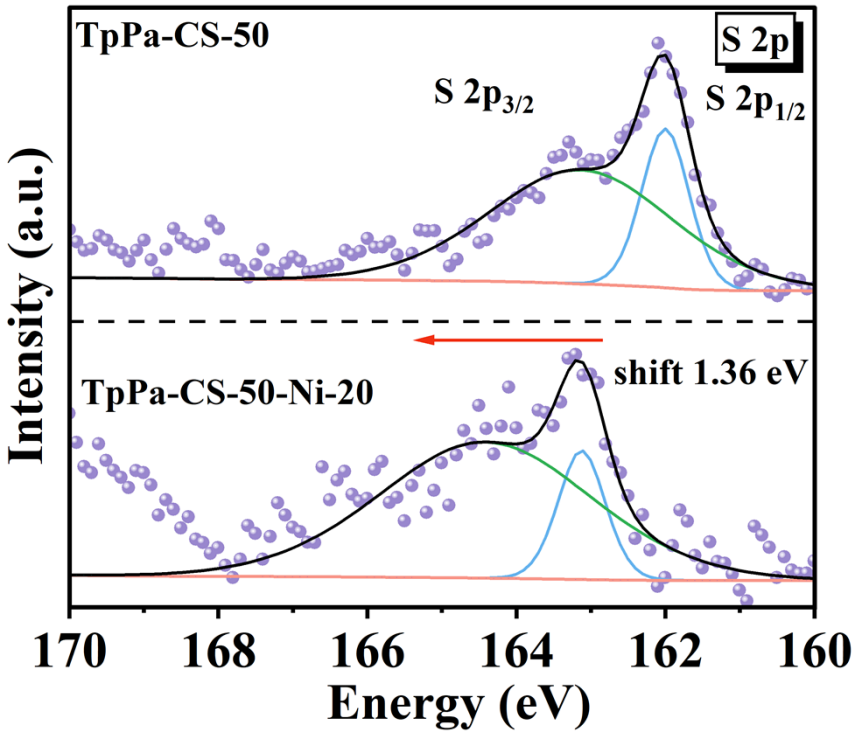

Fig. S19 XPS spectrum of S 2p of TpPa-CS-50 and TpPa-CS-50-Ni-20.

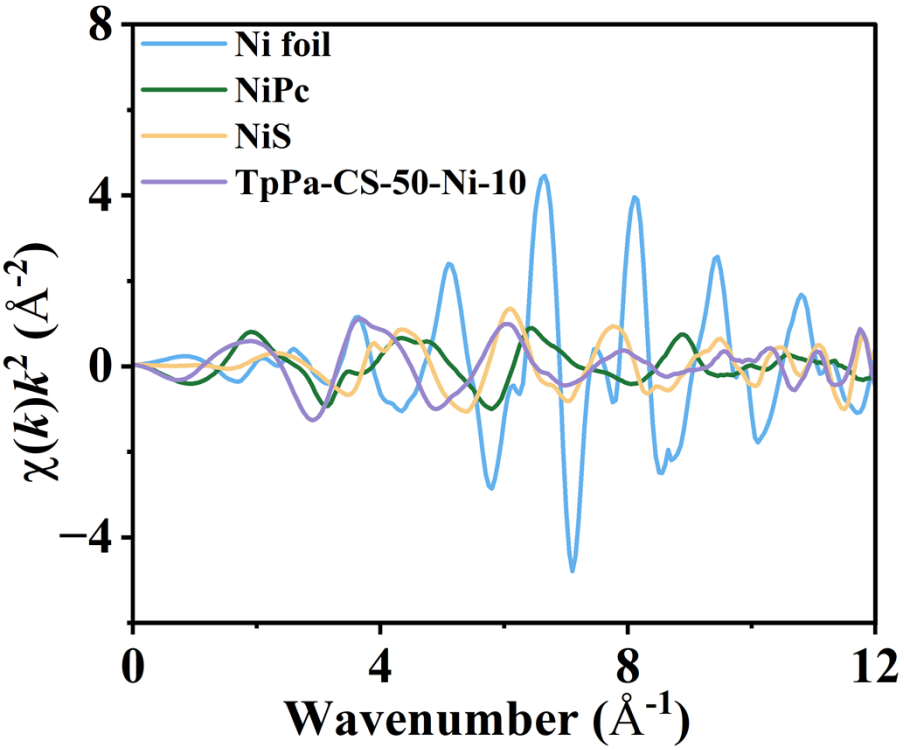

Fig. S20 EXAFS curves of Ni foil and NiPc and NiS and TpPa-CS-50-Ni-20 at k space.

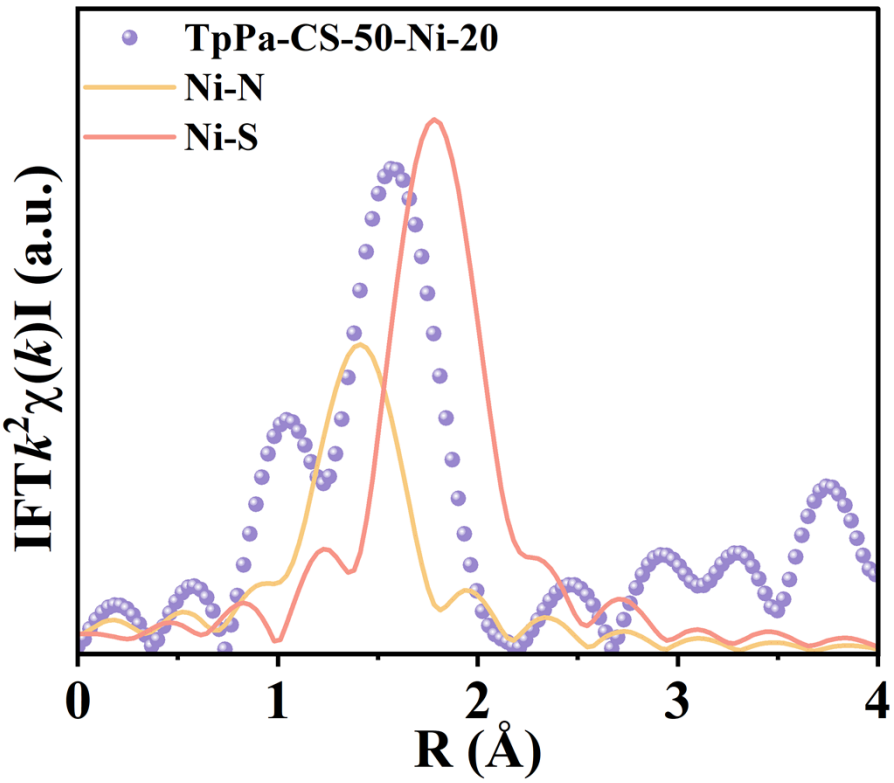

Fig. S21 EXAFS multiple-path fitting curves of TpPa-CS-50-Ni-20 at R space.

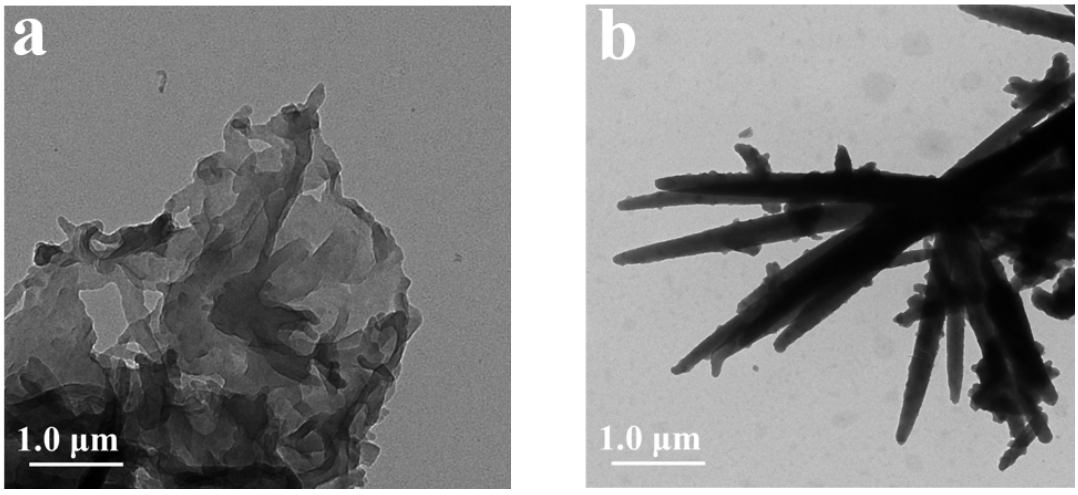

Fig. S22 TEM images of (a) TpPa and (b) TpPa-CS-50.

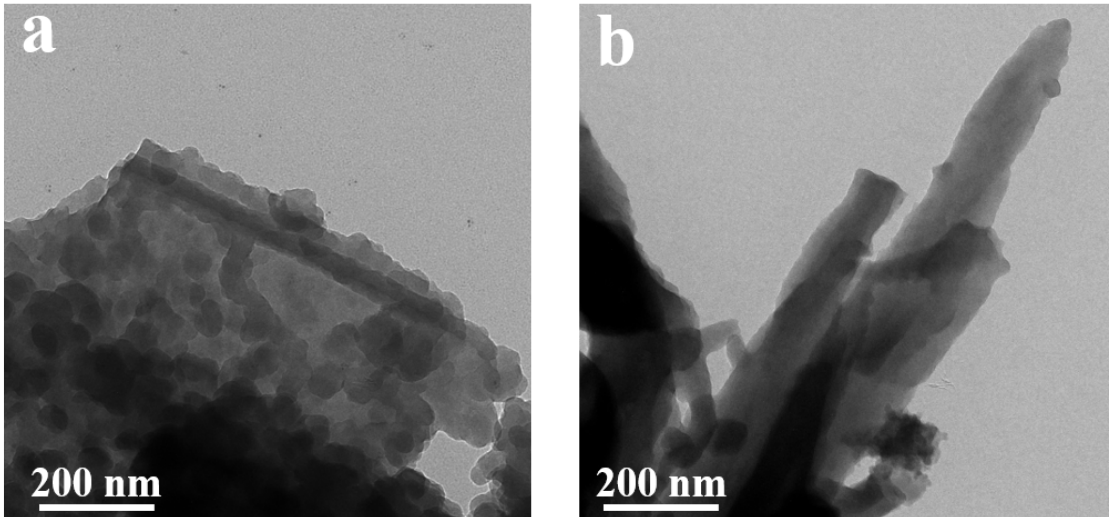

Fig. S23 TEM images of (a) TpPa-Ni-20 and (b) TpPa-CS-50-Ni-20.

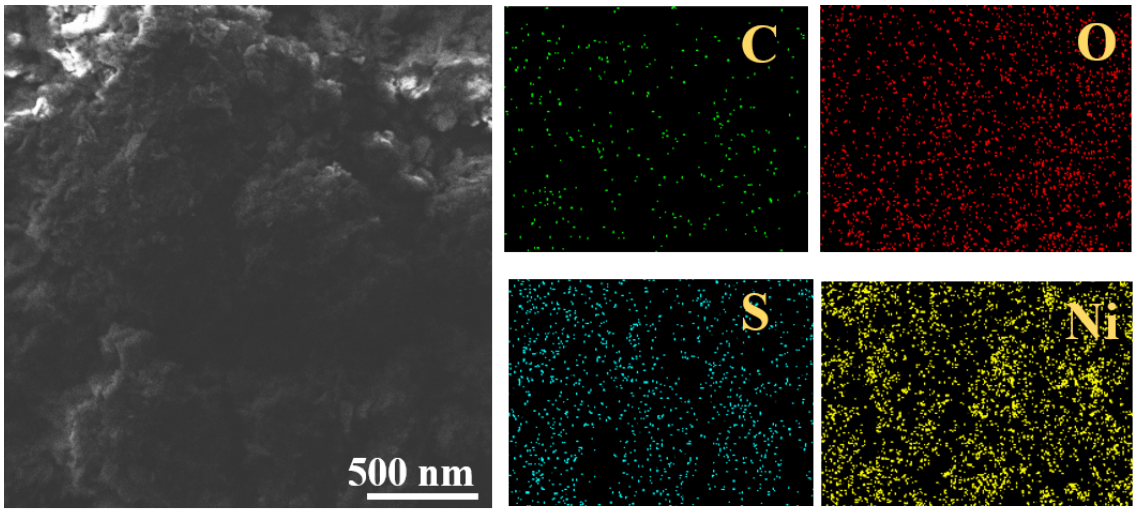

Fig. S24 EDS mapping of TpPa-CS-50-Ni-20.

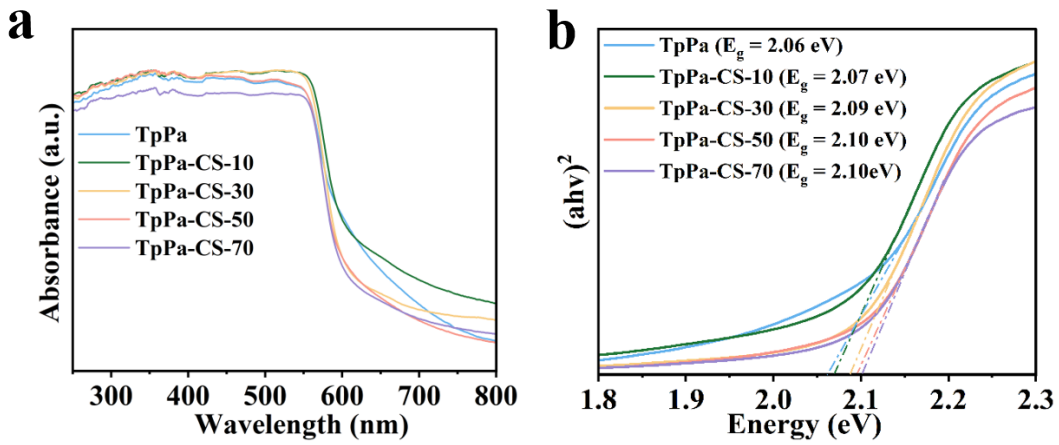

Fig. S25 (a) UV-vis diffuse reflectance spectra, (b) Tauc plot of and TpPa and TpPa-CS-X (X = 10, 30, 50 and 70).

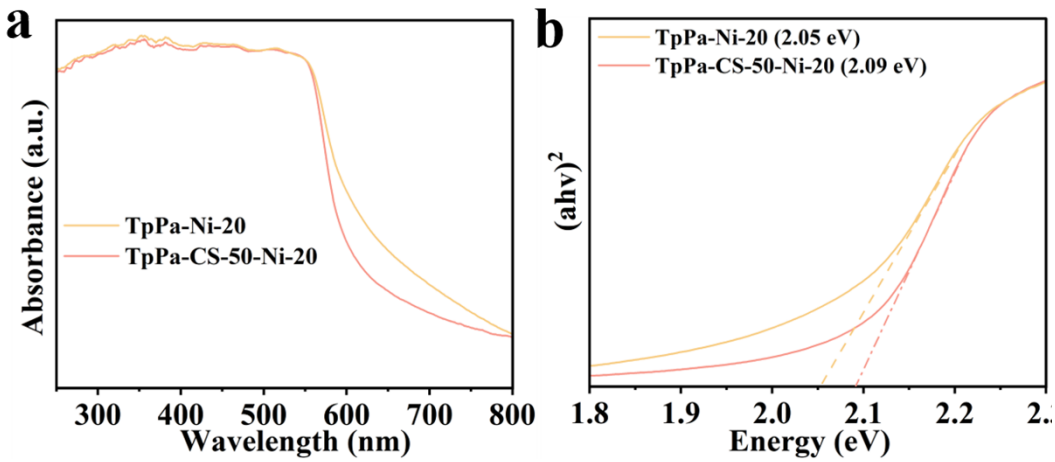

Fig. S26 UV-vis diffuse reflectance spectra (UV-DRS) (a) and Tauc plots (b) of TpPa-Ni-20 and TpPa-CS-50-Ni-20.

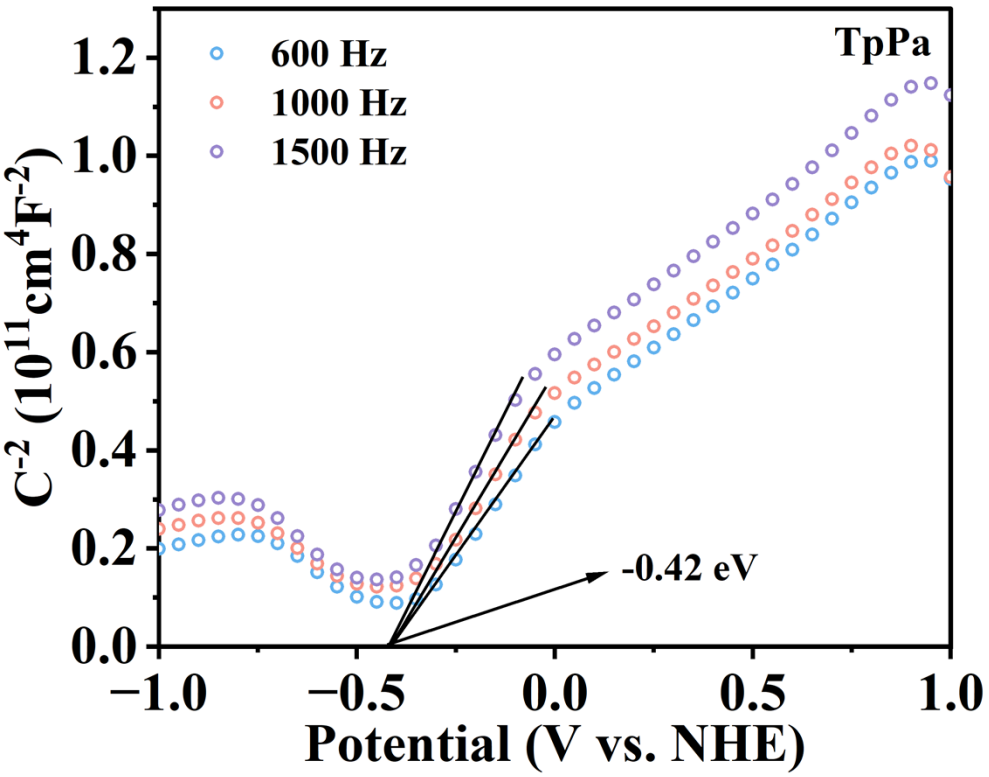

Fig. S27 Mott-Schottky plots of TpPa.

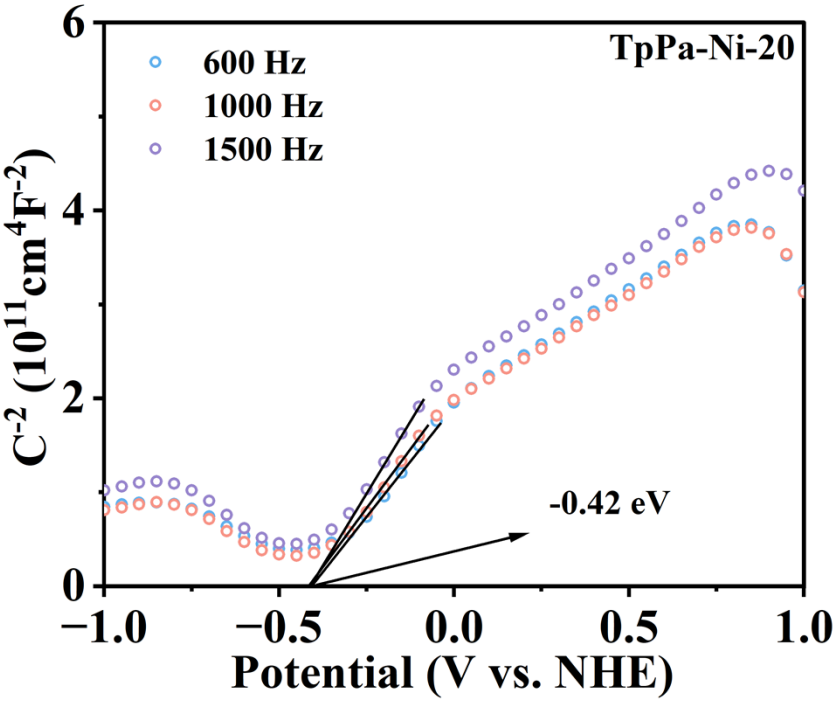

Fig. S28 Mott-Schottky plots of TpPa-Ni-10.

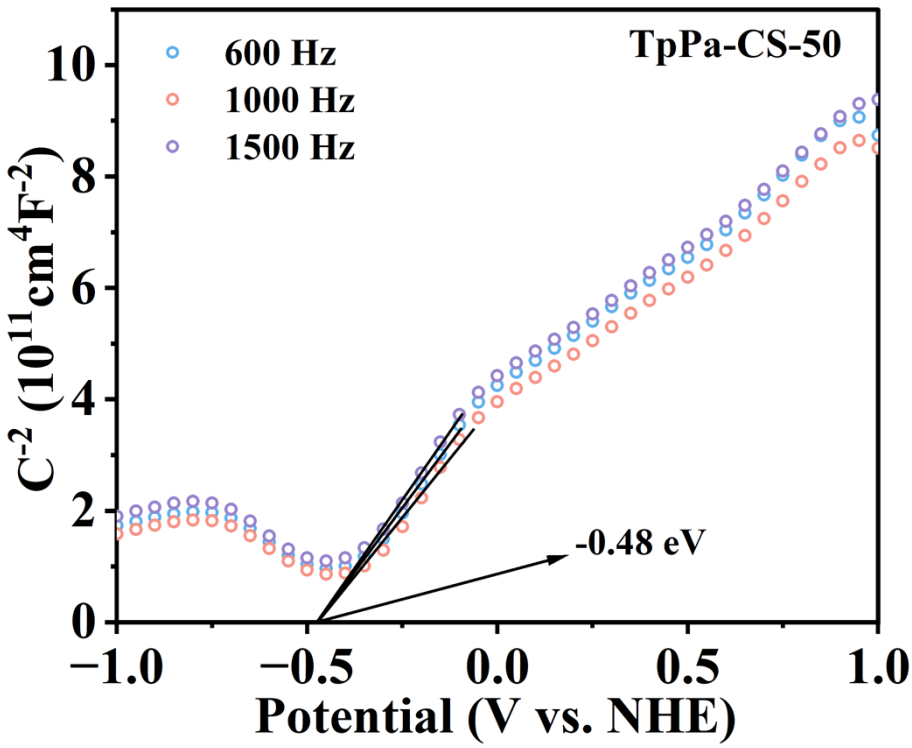

Fig. S29 Mott-Schottky plots of TpPa-CS-50.

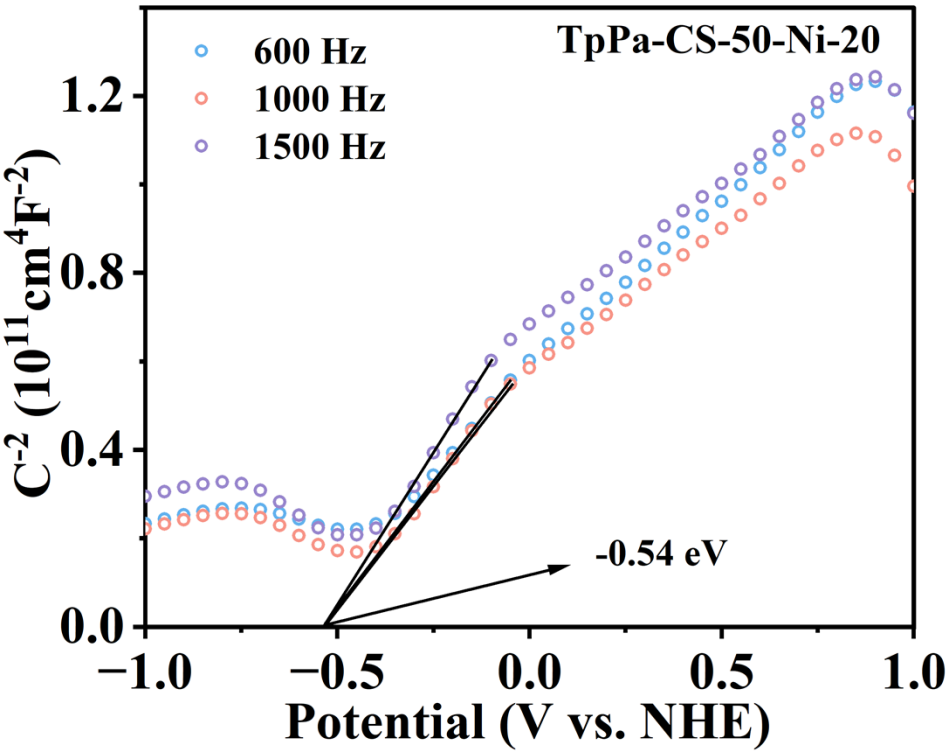

Fig. S30 Mott-Schottky plots of TpPa-CS-50-Ni-20.

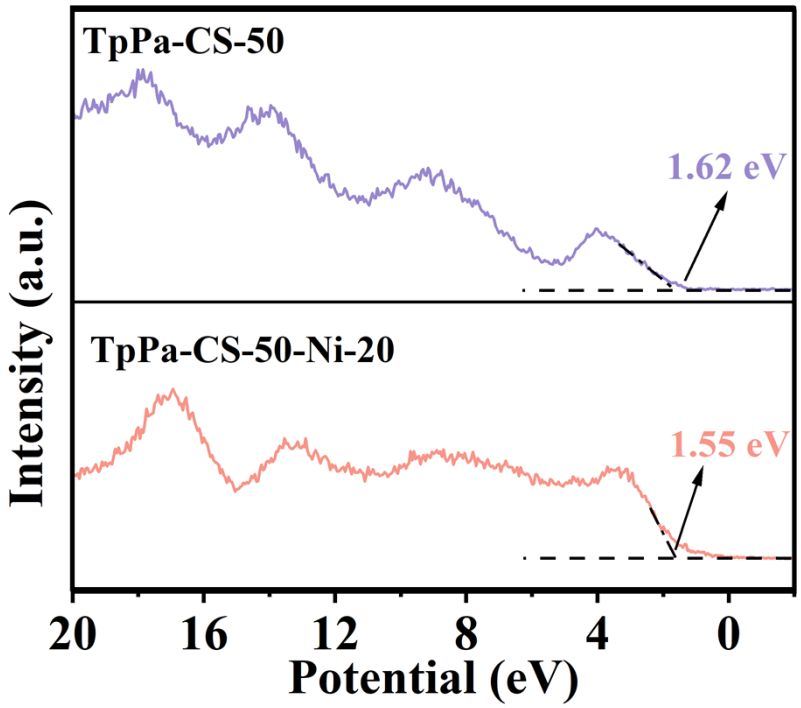

Fig. S31 XPS valence band spectra of TpPa-CS-50 and TpPa-CS-50-Ni-20.

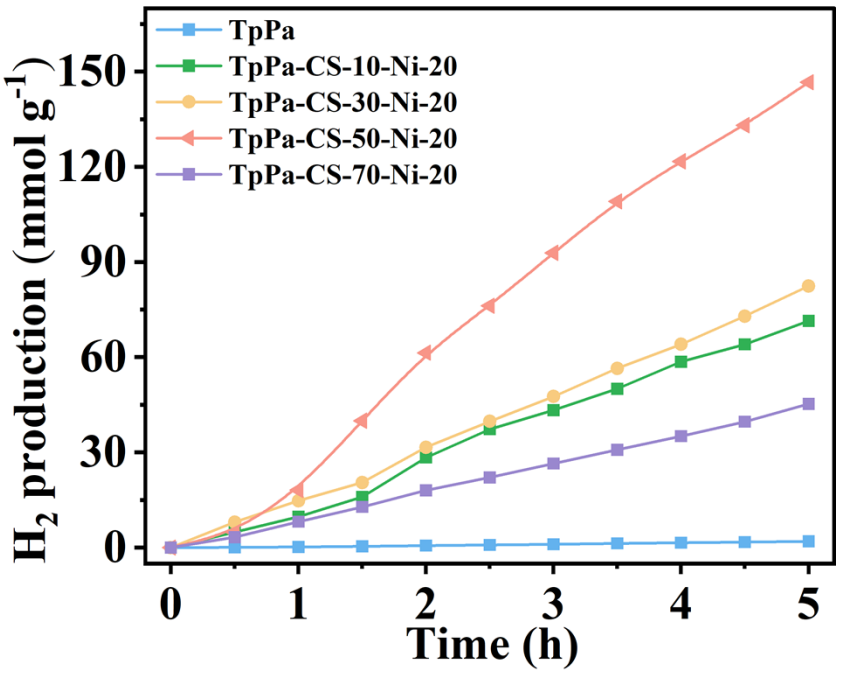

Fig. S32 Time profiles of photocatalytic hydrogen generation of TpPa and TpPa- CS-X-Ni-20 (X = 10, 30, 50 and 70).

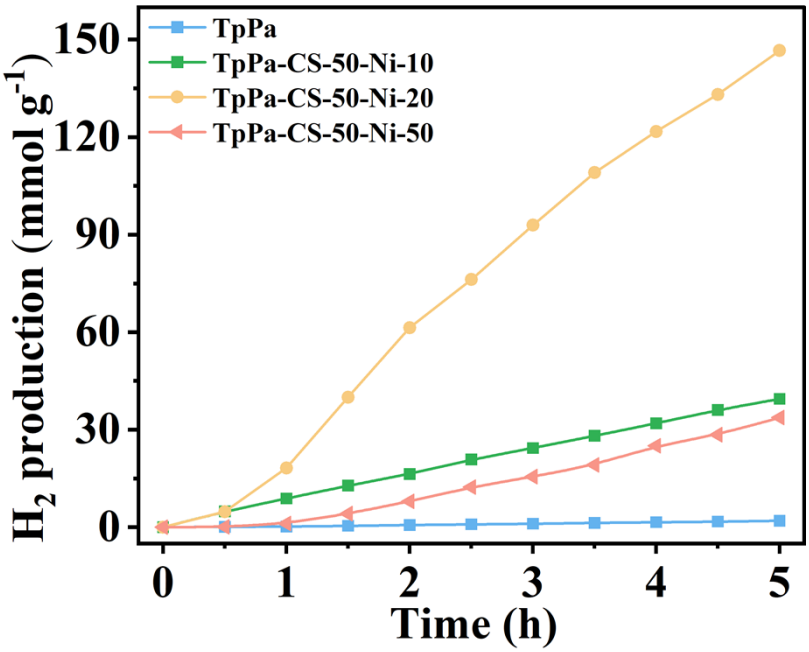

Fig. S33 Time profiles of photocatalytic hydrogen generation of TpPa and TpPa-CS-50-Ni-X (X = 10, 20 and 50).

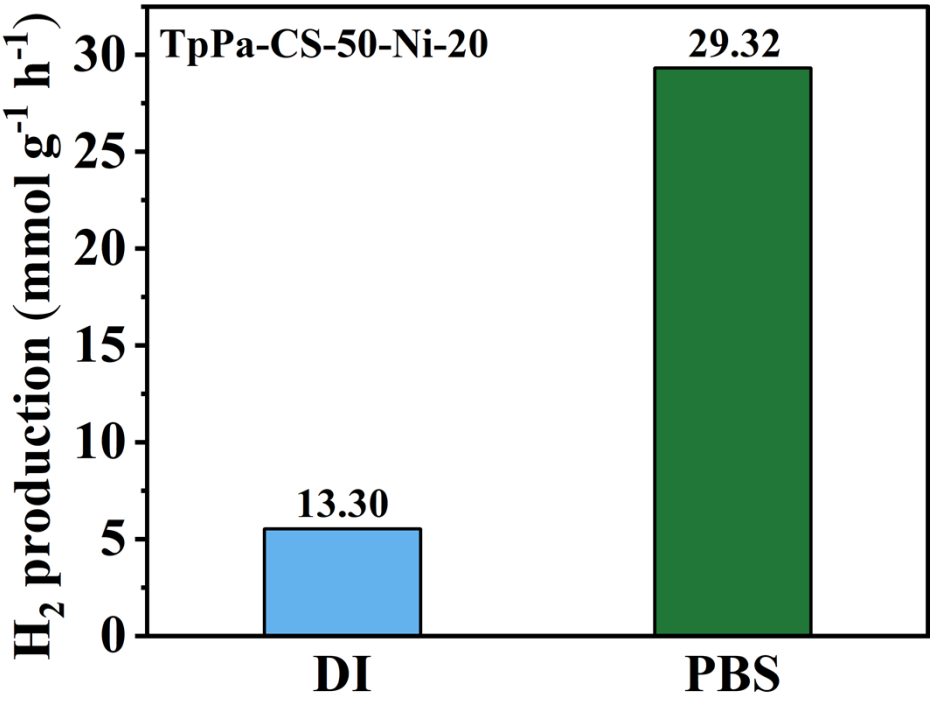

Fig. S34 The average hydrogen evolution rate of TpPa-CS-50-Ni-20 in two different solvents.

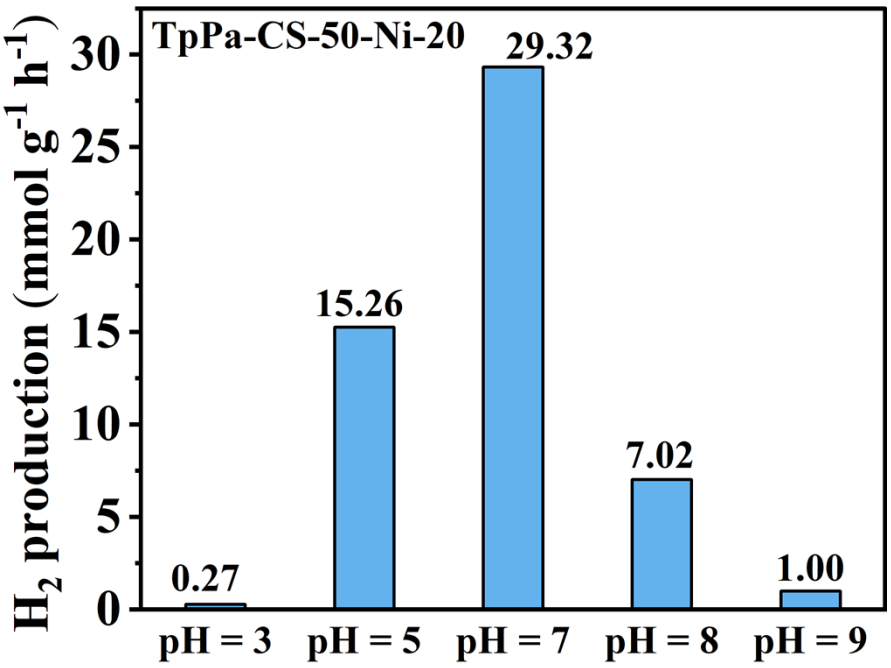

Fig. S35 The average hydrogen evolution rate of TpPa-CS-50-Ni-20 at different pH values.

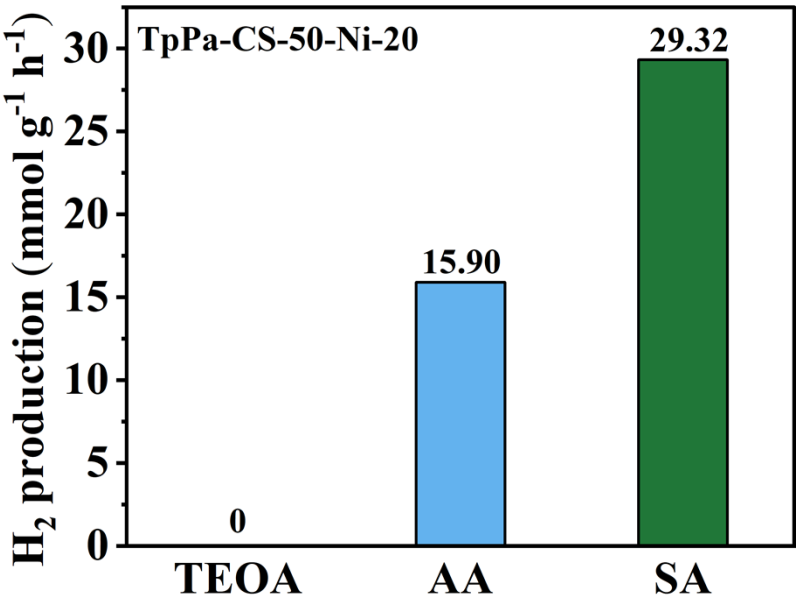

Fig S36 The average hydrogen evolution rate of TpPa-CS-50-Ni-20 using triethanolamine (TEOA), ascorbic acid (AA) and sodium ascorbate (SA).

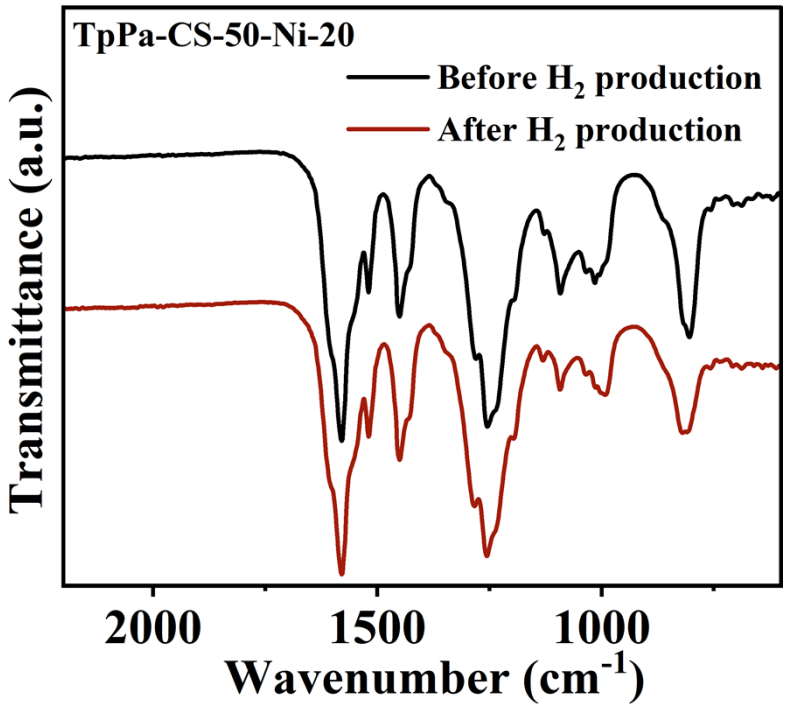

Fig. S37 FT-IR spectra of TpPa-CS-50-Ni-20 before and after photocatalysis.

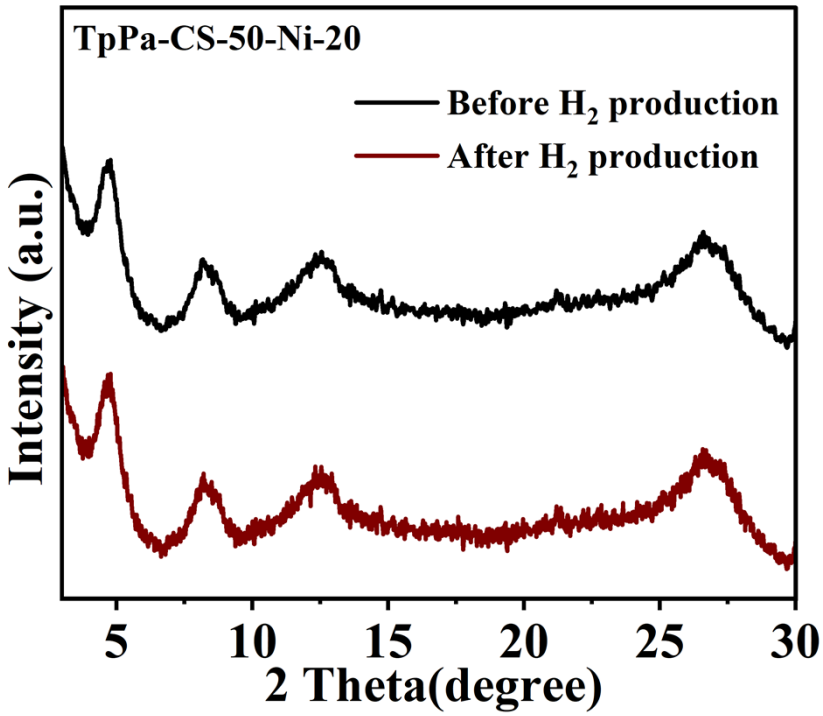

Fig. S38 PXRD patterns of TpPa-CS-50-Ni-20 before and after photocatalysis.

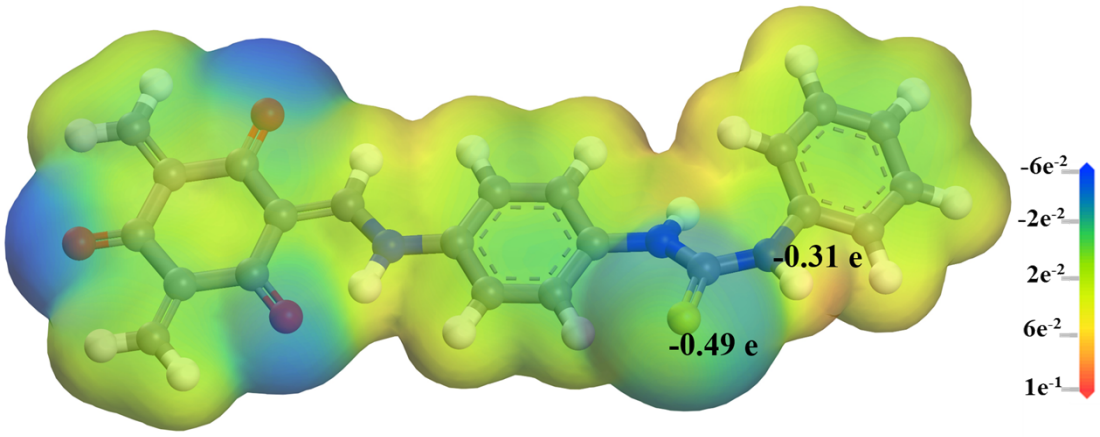

Fig. S39 Electrostatic potential distribution and Bader charge calculation results of TpPa-CS.

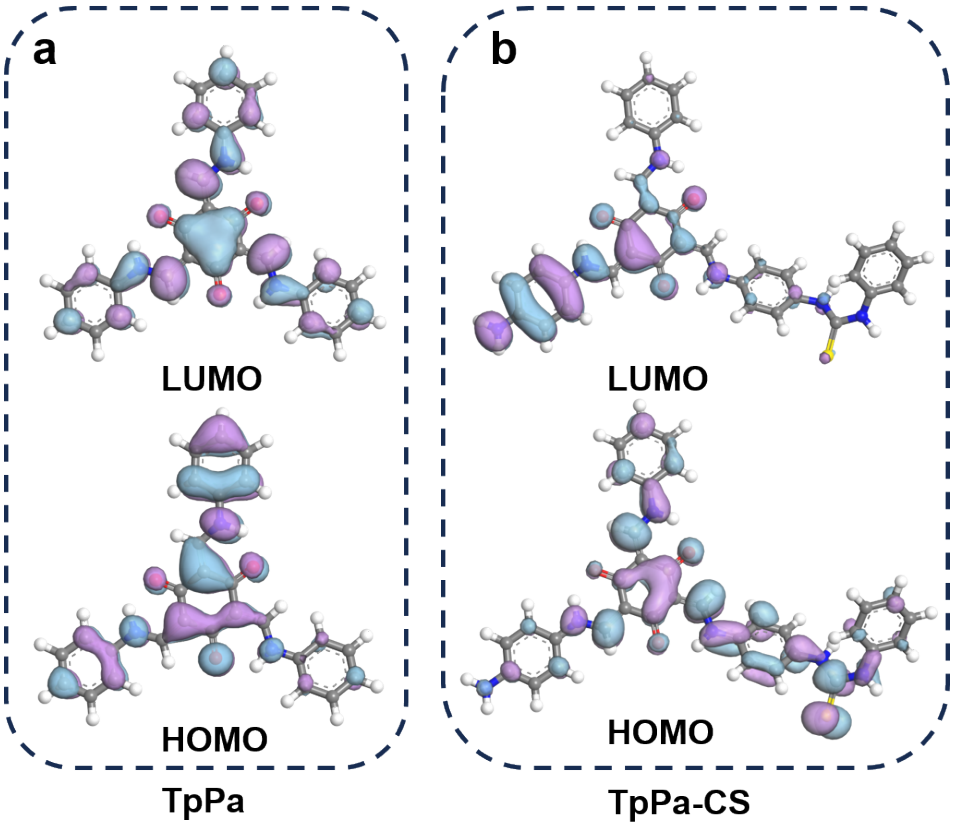

Fig. S40 LUMO and HOMO of (a) single-layer TpPa and (b) TpPa-CS.

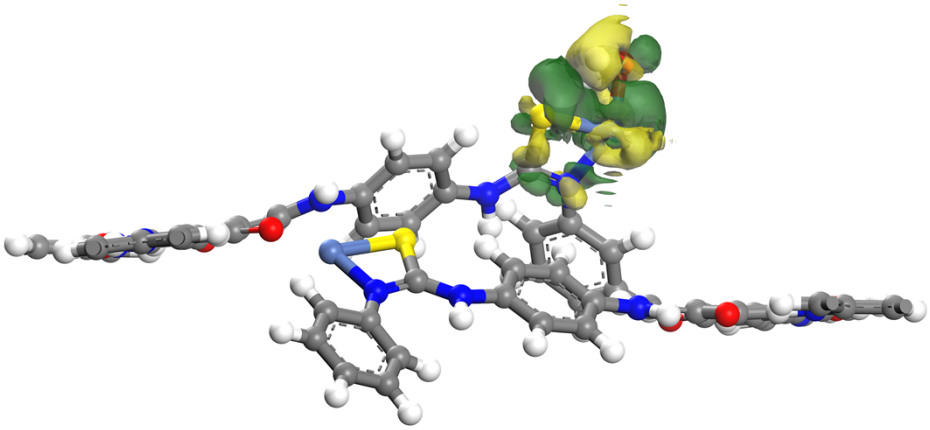

Fig. S41 Differential charge densities side view of TpPa-CS-Ni/H_2O.

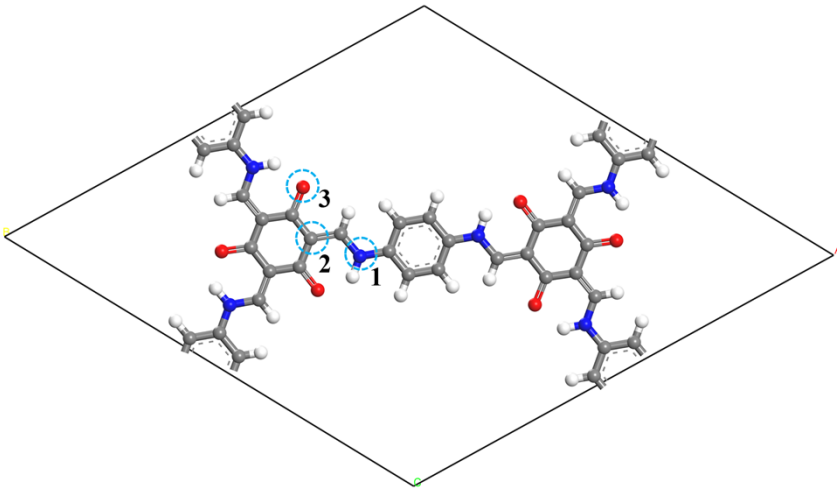

Fig. S42 Gibbs free energy active sites of TpPa.

Table S1 EXAFS fitting parameters at the Ni K-edge of TpPa-CS-50-Ni-20.

Bond type	CN	R (Å)	ΔE_0 (eV)	σ^2	R-factor
Ni-N	1.9	1.8	-15.24	0.00034	0.019
Ni-S	2.1	2.2		0.00367	

Table S2 Comparison of photocatalytic HER performance of reported composite COF materials.

Catalyst	Co-catalyst	Illumination	Amounts of catalyst (mg)	Activity ($\mu mol\ g^{-1}\ h^{-1}$)	Ref.
TpPa-CS-Ni	/	> 420 nm	2	29323	This work
Ni-Py-COF	Pt	> 420 nm	2	13231	S4
Ni-Bn-COF	Pt	> 420 nm	2	1805	
Ni-Py-COF	/	> 420 nm	2	626	
Ni-Bn-COF	/	> 420 nm	2	189	
ZnPor-DETH-COF	Pt	> 400 nm	2.5	413	S5
NiPor-DETH-COF	Pt	> 400 nm	2.5	211	
CoPor-DETH-COF	Pt	> 400 nm	2.5	25	
H_2Por-DETH-COF	Pt	> 400 nm	2.5	80	
Py-ClTP-BT-COF	Pt	> 420 nm	20	8875	S6
PyTz-COF	Pt	AM 1.5G	35	2072	S7
Sp^2c-COF	Pt	> 420 nm	50	1360	S8
Sp^2c-COF_{ERDN}	Pt	> 420 nm	50	2120	
NKCOF-108	Pt	> 420 nm	10	12000	S9
NKCOF-108	/	> 420 nm	10	50	
ACM-1	Pt	> 380 nm	40	1675	S10
TP-BPyN PCOF	Pt	> 420 nm	3	73656	S11
TP-BPyN PCOF	/	> 420 nm	3	306	
TpPa-1 (ST-HOAc)	/	> 420 nm	20	201	S12
Ni-COF-SCAU-1	/	> 420 nm	2	260	S13
RuCOF-TPB	Pt	> 420 nm	5	20308	S14
TpPa(Δ)-Cu(II)-COF	/	> 420 nm	10	14720	S15

Table S3 Fluorescence lifetime decay values obtained by exciting TpPa, TpPa-Ni-20, TpPa-CS-50 and TpPa-CS-50-Ni-20.

	B_1	τ_1/ns	B_2	τ_2/ns	B_3	τ_3/ns	τ_{avg}/ns
TpPa	2261.474	0.939	8593.076	0.939	1645.891	3.926	2.097
TpPa-CS-50	3971.731	0.784	7774.383	0.784	1154.330	3.634	1.675
TpPa-Ni-20	5123.987	0.729	7918.356	0.729	765.583	3.671	1.401
TpPa-CS-50-Ni-20	4372.624	0.712	8833.015	0.712	614.071	3.726	1.301

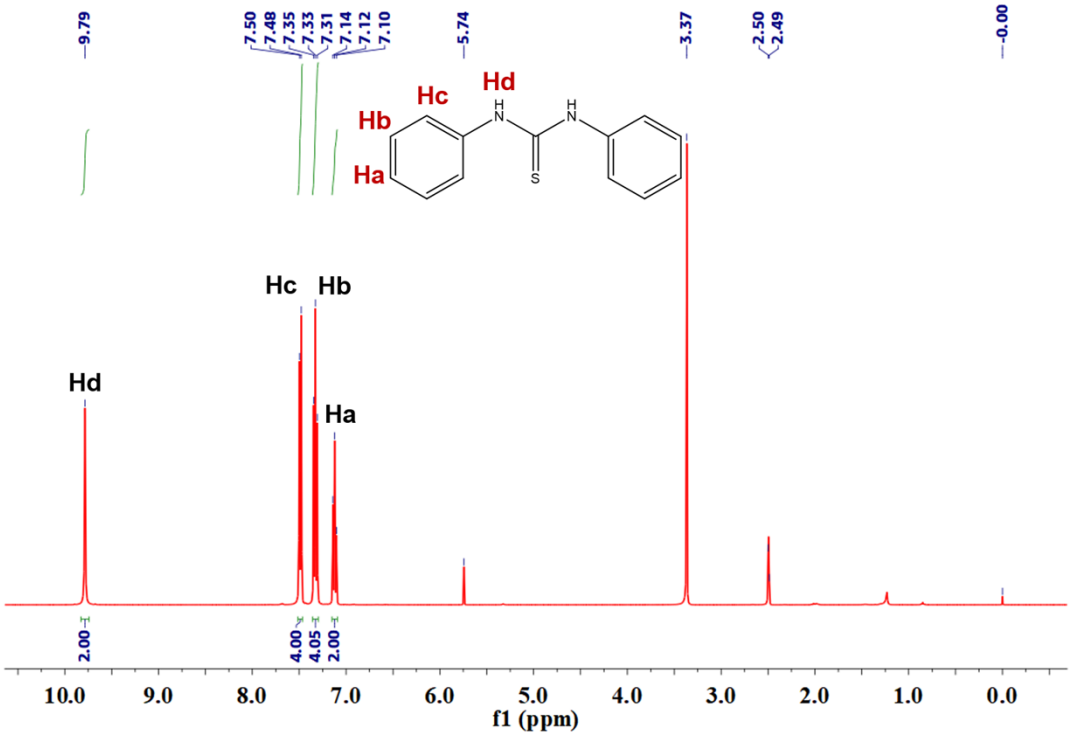

Fig. 43 ^{1}H NMR spectra for $(PhNH)_2CS$ in DMSO-d_6.

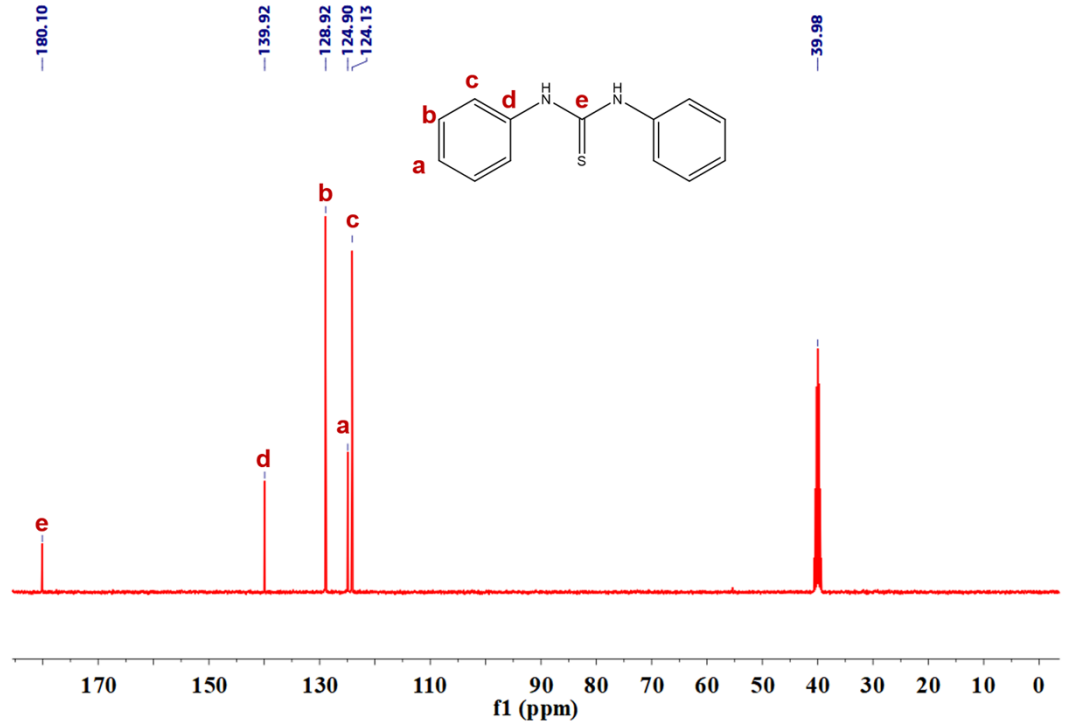

Fig. 44 ^{13}C NMR spectra for $(PhNH)_2CS$ in DMSO-d_6.

REFERENCES

S1 H. Yang, Y. Chen,; S. Suen and R. Lee, *Polymer*, 2023, **273**, 125853.

S2 W. Wu, Z. Li, S. Liu, D. Zhang, B. Cai, Y. Liang, M. Wu, Y. Liao and X. Zhao, *Angew. Chem. Int. Ed.*, 2024, **63**, e202404563.

S3 M. Samanta, H Tan, S. Laha, H. Vignolo-González, L. Grunenberg, S. Bette, V. Duppel, P. Schützendübe, A. Gouder, B. Yan and B. Lotsch, *Adv. Energy Mater.*, 2023, **13** 2300503.

S4 L. Sun, M. Lu, Z. Yang, Z. Yu, X. Su, Y. Q. Lan and L. Chen, Angew. *Chem. Int. Ed.*, 2022, **61**, e202204326.

S5 R. Chen, Y. Wang, Y. Ma, A. Mal, X. Y. Gao, L. Gao, L. Qiao, X. B. Li, L. Z. Wu and C. Wang, *Nat. Commun.*, 2021, **12**, 1354.

S6 W. Chen, L. Wang, D. Mo, F. He, Z. Wen, X. Wu, H. Xu and L. Chen, *Angew. Chem. Int. Ed.*, 2020, **59**, 16902-16909.

S7 W. Li, X. Huang, T. Zeng, Y. A. Liu, W. Hu, H. Yang, Y. B. Zhang and K. Wen, *Angew. Chem. Int. Ed.*, 2021, **60**, 1869-1874.

S8 E. Jin, Z. Lan, Q. Jiang, K. Geng, G. Li, X. Wang and D. Jiang, *Chem*, 2019, **5**, 1632-1647.

S9 Z. Zhao, Y. Zheng, C. Wang, S. Zhang, J. Song, Y. Li, S. Ma, P. Cheng, Z. Zhang and Y. Chen, *ACS Catal.*, 2021, **11**, 2098-2107.

S10 A. Cadiau, N. Kolobov, S. Srinivasan, M. G. Goesten, H. Haspel, A. V. Bavykina, M. R. Tchalala, P. Maity, A. Goryachev and A. S. Poryvaev, *Angew. Chem. Int. Ed.*, 2020, **59**, 13468-13472.

S11 X. Gao, J. Yuan, P. Wei, J. Dong, L. Chang, Z. Huang, H. Zheng, J. Liu, J. Jia and T. Luan, *ACS Catal.*, 2023, **14**, 533-546.

S12 P. Dong, C. Wang, L. Zhang, J. Pan, B. Zhang and J. Zhang, *ACS Catal.*, 2024, **14**, 17794-17805.

S13 R. Shen, X. Li, C. Qin, P. Zhang and X. Li, *Adv. Energy Mater.*, 2023, **13**, 2203695.

S14 W. K. Han, Y. Liu, X. Yan, Y. Jiang, J. Zhang and Z. G. Gu, *Angew. Chem. Int. Ed.*, 2022, **61**, e202208791.

S15 W. Weng and J. Guo, *Nat. Commun.*, 2022, **13**, 5768.